NANO LETTERS

2008
Vol. 8, No. 4
1033-1040

Microstructural Investigation of Magnetic $CoFe_2O_4$ Nanowires inside Carbon Nanotubes by Electron Tomography

Ovidiu Ersen,[†,*] Sylvie Bégin,[†] Matthieu Houllé,[‡] Julien Amadou,[‡] Izabela Janowska,[‡] Jean-Marc Grenèche,[§] Corinne Crucifix,[||] and Cuong Pham-Huu[‡]

Institut de Physique et Chimie des Matériaux de Strasbourg, UMR 7504 CNRS-ULP, 23 rue de Loess, 67087 Strasbourg, France, Laboratoire des Matériaux, Surfaces et Procédés pour la Catalyse, ELCASS, UMR 7515 CNRS-ULP, 25 rue Becquerel, 67087 Strasbourg, France, Laboratoire de Physique de l'Etat Condensé, UMR 6087 CNRS, Avenue Olivier Messiaen, 72085 Le Mans, France, and Institut de Génétique et Biologie Moléculaire et Cellulaire, UMR 7104, 1 rue Laurent Fries, 67404 Illkirch, France

Received October 21, 2007; Revised Manuscript Received January 28, 2008

ABSTRACT

Magnetic nanowires of $CoFe_2O_4$ were casted inside the channel of multiwall carbon nanotubes by mild chemical synthesis. A detailed investigation of these nanowires was performed using mainly the electron tomography technique; this study provides a complete characterization of their microstructure in terms of the spatial organization and the size distribution of individual particles forming the nanowire as well as its residual porosity. In particular, we have shown that the size of the $CoFe_2O_4$ monocrystalline particles is closely dependent on the location of the particle within the nanotube, i.e., small particles close to the tube tip (5 nm) and bigger particles inside the tube channel (15 nm). As the theoretical critical size for superparamagnetic relaxation in $CoFe_2O_4$ is estimated within the range of 4−9 nm, the size distribution obtained by 3D-TEM agrees with the Mössbauer study that suggests the presence of two different magnetic components inside the nanowire. We have shown also that, by using this preparation method and for this internal diameter of nanotube, the $CoFe_2O_4$ nanowire exhibits a continuous structure along the tube, has a residual porosity of 38%, and can fill the tube at only 50%, parameters which influence in a significant manner the magnetic behavior of this system.

Introduction. In the past decades, a significant scientific interest has been devoted to the study of confined (0D or 1D) nanomaterials, i.e., nanoparticles and/or nanowires, due to their unusual physical properties.[1] Magnetic particles and nanowires have received a considerable attention due to their potential employment in the fields of high-density magnetic storage devices (due to their size and anisotropic behavior, which permits the use of smaller bit size that favors the attainable recording density), contrast enhancers for magnetic resonance imaging, magnetic vectors for cell targeting and drug delivery, wiring materials for audio and radio frequency transformers, high-temperature space power systems, and catalysis.[2–4] Recent studies have also been focused on the synthesis of magnetic compounds with high aspect ratio using a template method, especially the anodic alumina template and multiwalled carbon nanotubes template.[5,6] Among these preparation methods, carbon nanotube templating seems to be the most employed to prepare nanowires with high selectivity for numerous potential applications.[7–10] Nanowires made of FeCo monocrystal were successfully made-up using a covaporization of a mixture of $FeCp_2$-$CoCp_2$-C_7H_8 solutions in an argon atmosphere at temperature ranged between 600 and 800 °C.[11] In our previous studies, nanowire materials were grown by the coalescence of several nanoparticles due to the imposed restriction of the surrounding rigid template, i.e., the nanotube wall.[12] Recently, $CoFe_2O_4$ nanowires were directly grown from a solution-based micelle method using a microemulsion medium.[13] The as-synthesized $CoFe_2O_4$ nanorods completely retained their morphology upon heating up to 720 °C. In addition, introduction of foreign elements inside the carbon tubules can give rise to peculiar effects either on the filling element or on the filled carbon nanotube. The challenge lying ahead concerns the easy control of the

* Corresponding author. E-mail: ovidiu.ersen@ipcms.u-strasbg.fr.
† Institut de Physique et Chimie des Matériaux de Strasbourg.
‡ Laboratoire des Matériaux, Surfaces et Procédés pour la Catalyse.
§ Laboratoire de Physique de l'Etat Condensé.
|| Institut de Génétique et Biologie Moléculaire et Cellulaire.

10.1021/nl072714e CCC: $40.75
Published on Web 03/13/2008

nanowire formation and the scalability of the process. However, up to now no microstructural investigation of these complex magnetic materials has yet been reported, even if their magnetic behavior is strongly dependent on their structural characteristics and organization. In particular, to fully understand the correlation between the morphology of the $CoFe_2O_4$ nanowire and its magnetic properties and stability, it is important to have access to its three-dimensional (3D) structure and, in particular, to physical parameters like the porosity inside the nanowire, the size distribution of the magnetic particles, or their crystallographic orientations and arrangement. For such investigation, electron tomography (or 3D-TEM) seems to be the most appropriate technique according to the previous results reported on other systems in the literature.[14–19] With respect to the classical TEM technique, it allows one to obtain volume-specific information on the nanomaterials having complex morphology or spatial distribution by using a series of TEM observations performed in a classical way.[20,21] In this general framework, the present work is devoted to the study of $CoFe_2O_4$ nanowires inside the multiwall carbon nanotubes (MWCNTs) channel obtained by mild chemical synthesis performed at relatively low temperature to avoid the excessive formation of carbide-like phases.[22–24]

The aim of the present communication is to report a detailed nanometric scale investigation of these casted $CoFe_2O_4$ nanowires by combining traditional characterization techniques such as XRD, Mössbauer, and magnetic measurements, and TEM tomography. This study provides a complete characterization of their microstructure in terms of their spatial organization, size distribution, and residual porosity with a resolution within the nanometer scale. With the 3D-TEM technique, it is thought that one will be able to access unprecedented information on the microstructural arrangement of the individual particles forming the nanowire and its relationship toward the magnetic behavior of this structure.

Experimental Section. Synthesis of the $CoFe_2O_4$ Nanowire inside CNTs. The $CoFe_2O_4$ nanowires were synthesized using commercial multiwalled carbon nanotubes (Pyrograf III) purchased from Applied Science, Ltd. (USA). TEM analyses indicated that the nanotubes were straight and had a relatively large inner channel (60 nm) with length up to several micrometers. These nanotubes were first cleaned by acid washing to remove as much as possible the remaining growth catalyst, then after drying they were treated at 800 °C for 2 h under flowing helium in order to remove all oxygenated groups from their surface. The O-to-C atomic ratio was tracked by XPS (results are available in the Supporting Information). Defunctionalized nanotubes were infiltrated by a mixture of metal precursor salts through an incipient wetness impregnation method. Cobalt nitrate ($Co(NO_3)_2$, $6H_2O$, 99%, ACROS) and iron nitrate ($Fe(NO_3)_3$, $9H_2O$, 99%, MERCK) were dissolved in the appropriate amount of water and ethanol (80:20 in volume). The previous solution was added to the treated nanotubes until a paste-like mixture was obtained, and then the solid was left to dry overnight at room temperature. Some of these nanotubes were set aside to be heated directly in air at 100 °C at a rate of 1 °C/min. The remaining nanotubes were loaded in a tube furnace to be heated respectively at 400 and 600 °C under Ar atmosphere (1 °C/min) and kept at these temperatures for 2 h.

Characterizations. Zeta potential measurements and pH titrations were carried out on a Nano-ZS (multipurpose titrator, Malvern Instruments). Samples were sonicated in $NaClO_4$ aqua solution for 30 min before measurements. Titrations of the CNTs were performed using NaOH and HCl aqueous solutions. The ζ potential values were determined from the particle velocities according to the Helmholtz−Smoluchowski equation: $\zeta = 4\pi\mu\eta/D$ where μ is the electrophoretic mobility, η is viscosity, and D the dielectric constant of the liquid in the boundary layer. The X-ray powder diffraction (XRD) patterns were recorded on a Bruker diffractometer (D8 Advance) with Cu Kα radiation in a 2θ range from 20° to 80°. Transmission Mössbauer spectrometry was carried out by means of a bath cryostat, using a constant acceleration spectrometer and a ^{57}Co source diffused into a Rh matrix. The in-field spectrum was obtained using a cryomagnetic device where the external field is applied parallel to the γ-radiation. The values of the isomer shifts are quoted relative to a $\alpha-$Fe foil at 300 K. The hyperfine parameters were refined from a model involving components composed of Lorentzian lines using a least-squares fitting procedure in MOSFIT program. Magnetic measurements were performed on a vibrating magnetometer (Foner VSM). The HRTEM measurements were performed on a Topcon 002B microscope with an acceleration voltage of 200 kV and a point-to-point resolution of 0.18 nm.

The 2D experimental images for 3D-TEM were recorded in bright-field mode on a F20 TECNAI microscope (FEI Company) using an acceleration voltage of 200 kV and a high-tilt sample holder. For our samples, the diffraction contrast in the BF images remains relatively low and thus we can consider that the recorded images of the tilt series fulfill the projection requirement. Before acquisition, a drop of solution containing calibrated gold nanoparticles (5 nm) was deposited onto the holey grid supporting the sample to ease the alignment procedure before reconstruction. Several tilt series were acquired with automatic rectification (correction of the focus and the horizontal displacement) using the FEI Explore 3D acquisition software on a 2048 × 2048 pixel cooled CCD array detector. The tilt range was set from −65° to 65°, with an image recorded every 2° between –35° and 35° and respectively every 1° elsewhere, giving a total of 96 images. After a fine alignment of all projections, the volume reconstruction was calculated by the weighted back-projection algorithm implemented in the IMOD software from University of Colorado.[25] With our acquisition parameters and the geometrical characteristics of the specimen under study, the spatial resolutions in our tomogram is about 1.5 nm in the directions perpendicular to the electron beam and 2 nm in the parallel direction due to the presence of a missing wedge related to the limited tilt angle.[26] To model the as-obtained volume and estimate the quantitative parameters, we finally used a segmentation procedure based on the gray-level intensities of the voxels. More details on the

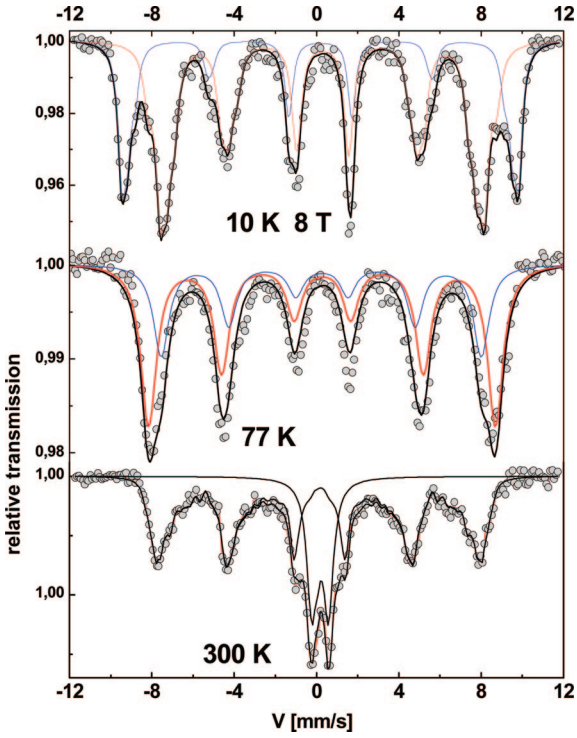

Figure 1. Mössbauer spectra of the $CoFe_2O_4$ nanowires recorded at 300, 77, and 10 K under 8 T external field (the blue and red lines correspond to tetrahedral and octahedral iron sites, respectively).

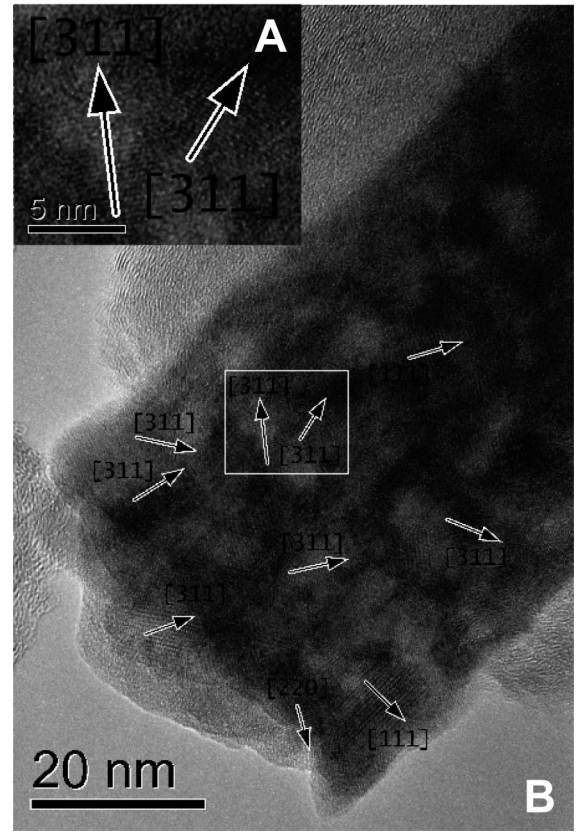

Figure 2. HRTEM image of the extremity of the $CoFe_2O_4$ nanowire. The interplanar distances obtained confirm the nature and stoichiometry of the mixed oxide. Inset: Zoom corresponding to the white square on Figure 2A showing the random orientation of two adjacent monocrystalline areas.

experimental setup and volume reconstruction and analysis in 3D-TEM technique can be found elsewhere.[19,20]

Results and Discussion. Support and Nanowire Characterizations. To follow the influence of the surface treatments on the charge surface of the carbon nanotubes, ζ potential measurements were performed at each step. Zeta potential curves are provided as Supporting Information (Figure SI1). The isoelectric point (IEP) of the starting CNTs (pH at which the ζ potential is zero) is around 3.8. The acid-treated CNTs display a negative ζ potential value (-55 to -40 mV) over the entire pH range, conducting to a higher stability in suspension than defunctionalized CNTs[27–30] and showing that these CNTs present a high density of acidic sites. The curve after defunctionalization of the CNTs is very close to the one of pristine CNTs, suggesting a low level of impurities in the raw CNTs. The IEP of defunctionalized CNTs is around 3, meaning that the ζ potential value is positive at the pH of infiltration process, ca. pH = 1.5. Thus there will be repulsion interactions between the nanotube surface and the Co and Fe cations during the infiltration process, which will inhibit outer surface deposition of the ferrite phase. Similarly, the use of acid-treated CNTs would lead to a both inner and outer surface deposition of the metal phase (See Supporting Information (Figure SI2) for additional data). Defunctionalized CNTs were subsequently infiltrated by a known amount of Co and Fe nitrate solution and left to dry at room temperature. A heat treatment at 400 °C under Ar was then performed in order to induce a liquid-to-solid transformation. According to TEM results, the CNTs were filled with a $CoFe_2O_4$ phase, and no trace of Co or Fe were detected on the outside walls of CNTs (see Supporting Information, Figure SI3B). Considering the surface charge, the capillary forces were mainly responsible for the filling owing to the relatively low surface tension of the solution and the large inner diameter of the nanotubes, thus leading to complete and selective filling.

Preliminary analyses were performed by XRD and Mössbauer spectrometry in order to verify the formation of the $CoFe_2O_4$ oxide. In particular, the crystallinity of the material after air calcination at 100 °C and thermal treatment in flowing argon at 400 °C was examined by X-ray diffraction (XRD) and the corresponding results are supplied as Supporting Information (Figure SI3A). The diffraction peaks can be indexed as those belonging to the $CoFe_2O_4$ cubic phase.[13] No impurity peaks were detected in the XRD pattern, indicating the high purity of the sample. The average particle size calculated by the Scherrer formula was about 8 nm, which is in the range of magnetic particles that exhibit maximum coercivity.[31]

To study the formation of cobalt ferrite, Mössbauer spectrometry was performed on the sample at 300 and 77 K: the two resulting spectra are shown in Figure 1. At 300 K, our sample exhibits two components: a magnetic sextet and a quadrupolar doublet, while only a magnetic hyperfine structure is observed at 77 K. The asymmetry of the 77 K spectrum can be described by means of two sextets with mean hyperfine fields of 52.0(5) and 48.0(5) T with propor-

tions of 62 ± 5 and 38 ± 5%, respectively; according to the different isomer shift values (0.47(1) and 0.40(1) mm/s respectively), these two components can be ascribed to the presence of only Fe^{3+} ions located in octahedral and tetrahedral sites, respectively, allowing one thus to confirm the formation of $CoFe_2O_4$. One can note that the hyperfine parameters are consistent with those encountered in the literature.

In addition to the nonpresence of Fe^{2+} ions, one can *a priori* conclude an inverse spinel structure with a small cationic inversion but the lack of resolution of the hyperfine structure prevents an accurate estimation of the relative spectral absorption. Consequently, the proportions of each Fe site have been carefully estimated by means of in-field Mössbauer experiments: an 8 T external field allows two broadened line sextets to be distinguished, in agreement with the ferrimagnetic structure. Then the proportions of tetrahedral and octahedral Fe sites (accurately estimated at 33 ± 1% and 67 ± 1%, respectively) thus confirm the $(Fe^{3+})_A(Co^{2+}Fe^{3+})_BO_4$ structure (without cationic inversion). Moreover, the intermediate line intensities of each component suggest a canting of Fe^{3+} ions estimated at about 30° for Td sites and 48° for Oh sites. Such canting has already been observed in nanosized $CoFe_2O_4$ nanoparticles and attributed to surface effects.[32] At 300 K, the presence of both a quadrupolar doublet and a magnetic sextet with an asymmetric line profile suggests the existence of superparamagnetic phenomena with different relaxation times. They originate from the nanowire structure made of magnetic particles and noninteracting smaller particles. Such a view is consistent with the first TEM images.

Although the theoretical critical size for superparamagnetic relaxation in $CoFe_2O_4$ is not known, other works have shown that it should be within the range of 4−9 nm.[33–35] The wide particle size distribution in our sample may explain why it exhibits two different magnetic components. From the area ratio of the quadrupole doublet to the split sextet, the fraction of particles showing superparamagnetic behavior can be determined: about one-third of the particles have size below the superparamagnetic critical value.

Magnetic nanowires or nanoparticles could be used in several fields of technology going from high-density information storage, ferrofluid technology, radar-absorbing coatings, MRI, or hyperthermia therapy. To be effective in these domains, the synthesized materials should belong to a given range of particle size[31] and have a significant magnetic signal. Magnetization measurements were performed on the as-synthesized $CoFe_2O_4$ nanowires: magnetization of the sample treated at 400 °C was recorded as a function of the applied magnetic field at room temperature and at 5 K. The results are supplied as Supporting Information (Figure SI4). A hysteresis loop is observed at room temperature, showing that the global magnetic behavior is not superparamagnetic. No saturation of the magnetization has been evidenced, which means that the nanowire is made of small magnetic particles that cannot all be saturated by the external magnetic field at room temperature. The corresponding maximum magnetization (M_{max}), remanent magnetization (M_r), and coercivity (H_c) at room temperature were 13 emu/g, 2.4 emu/g, and 330 Oe, respectively, while at 5 K, the saturation magnetization decreased down to 8 emu/g and the coercivity increased significantly up to 13500 Oe. These results are characteristic of single-domain cobalt ferrite nanoparticles and are similar to those observed by other authors.[36–39] The very large coercivity and low saturation magnetization at 5 K are consistent with a local magnetic anisotropy coming from Co^{2+}, inhibiting the alignment of the moment in the applied field,[40,41] in agreement with the features previously established from the in-field Mössbauer spectrum. The reduced remanence M_r/M_s at 5 K, slightly higher than 0.5, suggests randomly orientated equiaxial particles with cubic magnetocrystalline anisotropy. On this curve is also observed a dissymmetric hysteresis indicating a ferromagnetic coupling with a magnetically hard material. Muroi et al.[42] have attributed it to core–shell particles with a ferrimagnetic core and a spin glass shell that are exchange coupled. This hypothesis would be consistent with the spin canting observed by Mössbauer spectrometry under an applied field. The low fraction of superparamagnetic nanoparticles ($^1/_3$), the size distribution, which induces a distribution of the blocking temperatures, the magnetocrystalline and surface anisotropies, and the interparticle interactions may increase the blocking temperature and mask their size dependence. Such size distribution within the cobalt ferrite nanowire was investigated in details by electron tomography as presented below.

The induced magnetic behavior of ferrimagnetic nanowires is obviously strongly related to their geometrical shape, residual porosity, and to the spatial organization of the nanoparticles constituting the nanowire. A rough estimation of these parameters is requested for the optimization of the magnetic properties in the applications presented here above. A preliminary analysis of the morphology and crystallographic structure of these composite samples was performed by TEM in bright-field and high-resolution mode (a typical image of a $CoFe_2O_4$ nanowire recorded in bright-field mode is available in Supporting Infomation Figure SI3B). According to this image, the granular morphology of the nanowire can clearly be evidenced by the presence of a high proportion of residual pores corresponding to bright zones. It is notable that the nanowire morphology was not modified during the heat treatment process, i.e., from 100 to 400 °C.[5] Apparently, the crystallization took place in a continuous manner, i.e., coalescence of the neighboring nanoparticles along with the release of gaseous NO_x and H_2O without breaking of the initial morphology. Such local aggregation will be described and discussed in details below using the 3D-TEM reconstructed object. High-resolution TEM analyses were performed at different positions of the nanowire, and an example of typical image is presented in Figure 2. The granular morphology of the nanowire is once again visible in this image. The parallel fringes corresponding mainly to the (311) crystallographic planes of $CoFe_2O_4$ are also visible in many areas of the nanowire. However, no relationship between these different crystallographic orientations could be evidenced. We can conclude here that the

magnetic nanowires contain monocrystalline areas of $CoFe_2O_4$, randomly oriented, with average sizes between 5 and 15 nm. Terrones and co-workers[11] have successfully synthesized CoFe nanowires made of single crystals cast inside the carbon nanotube channel by coevaporation of a mixture of $FeCp_2$-$CoCp_2$-C_7H_8 in an argon flow at 800 °C on a quartz substrate. The difference in the crystallinity between the CoFe and the $CoFe_2O_4$ nanowires in this work could be attributed to the lower thermal treatment, i.e., 400 °C instead of 800 °C. It is noteworthy that $CoFe_2O_4$ nanowires consisting in a stacking of several $CoFe_2O_4$ single crystals along the nanowire axis can be obtained after heat treating the sample in flowing argon at 600 °C for 2 h (not shown).

Zhang et al.[13] have reported similar observation during the HRTEM investigation of self-supported $CoFe_2O_4$ nanowires after calcination up to 720 °C. According to these results, the $CoFe_2O_4$ nanowire could be made of several individual magnetic nanocrystals bonded to each other but without global orientation. Yet, as the recorded images are in fact planar projections of the whole sample, it is almost impossible to get more information on the porosity, particle size distribution, or arrangement of the magnetic particles within the nanowire. A quantitative determination of these geometrical characteristics is requested in order to be able to predict and optimize the magnetic properties of these confined systems. With this aim in view, we use the ability of 3D-TEM technique to extract 3D specific information about samples having complex morphology, structure, and self-organization at the nanometer scale.

Microstructural Characterization of the Nanowire by 3D-TEM. A typical 2D-TEM image (in bright-field mode) from the tilt series used for the volume reconstruction is presented in Figure 3A. Three successive longitudinal sections through the reconstructed volume of the same sample are also presented (Figure 3B−D). Generally speaking, an increase of the signal-to-noise ratio in the sections with respect to the initial projections can be observed due to the redundancy of information coming from several images.[43] According to these sections, the presence of a high proportion of residual porosity can be observed once again along the tube axis. However, it is noteworthy that such porosity is almost impossible to quantify using traditional TEM images (Figure 3A versus Figure 3B−D) due to the overlapping of the different magnetic nanoparticles and porous area in the projected image. A careful examination of the microstructure of the different $CoFe_2O_4$ nanoparticles inside the nanowire reveals that this latter was constituted by several series of chain-like nanoparticles with an orientation almost parallel to the longitudinal axis (Figure 4). These chain-like nanoparticles were thought to be formed during the heat treatment process by coalescence of nearby particles. Such peculiar assemblies could be explained by the decomposition of gaseous products, which induce a preferential channel inside the longitudinal axis when escaping.

The average $CoFe_2O_4$ particle size was determined by measurement of several representative particles from the transverse and longitudinal 3D-TEM slices. We underline

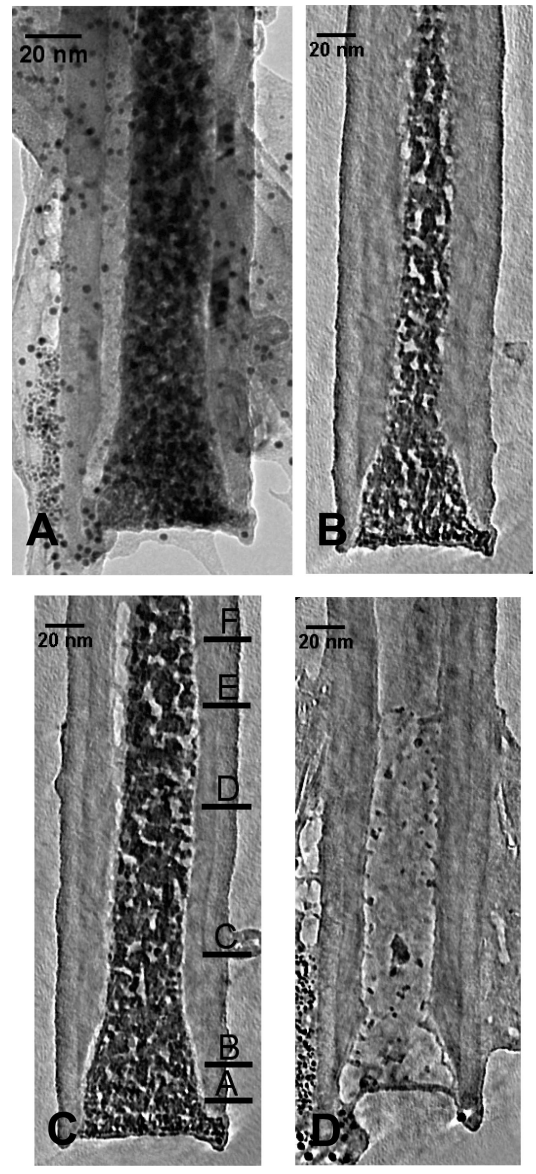

Figure 3. (A) Typical 2D-TEM image of the $CoFe_2O_4$ nanowire casted inside the carbon nanotube. (B,C,D) Three longitudinal sections through the volume reconstruction of the whole system showing the presence of a highly porous structure.

here that, with respect to a typical 2D-TEM image, what is particularly new from 3D-TEM analysis is the possibility to analyze in an individual manner the different components (here, the $CoFe_2O_4$ particles) of the sample under study. We observed that the mean size estimated at different z-positions along the tube axis was significantly different depending on their location within the nanowire (Figure 5).

$CoFe_2O_4$ particles located next to the tube tip are characterized by sizes centered at around 5 nm, whereas their size slowly increased while going deeper inside the tube tubule, i.e., 15 nm. Such results could be attributed to variations of the local pressure along the tube axis during the liquid-to-solid reaction: the high surface front of the liquid located next to the tube tip should allow the rapid and uniform evaporation of the liquid leading to the formation of smaller particles.[29] While at deeper distance from the tube tip, the restricted evacuation of nitrogen oxides produced during the

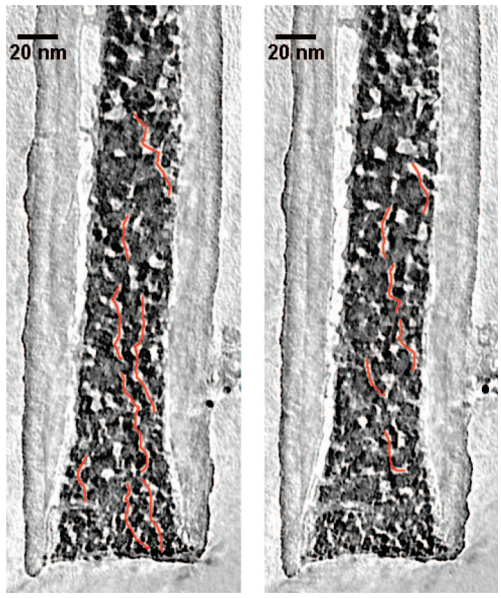

Figure 4. Two typical sections through the reconstructed volume. In red are marked the channels through which gaseous products evacuate the nanotube during the nitrate decomposition. These evacuation canals induce the formation of chain-like aggregates owing to the coalescence of neighboring nanoparticles and tend to form a network oriented along the nanotube axis.

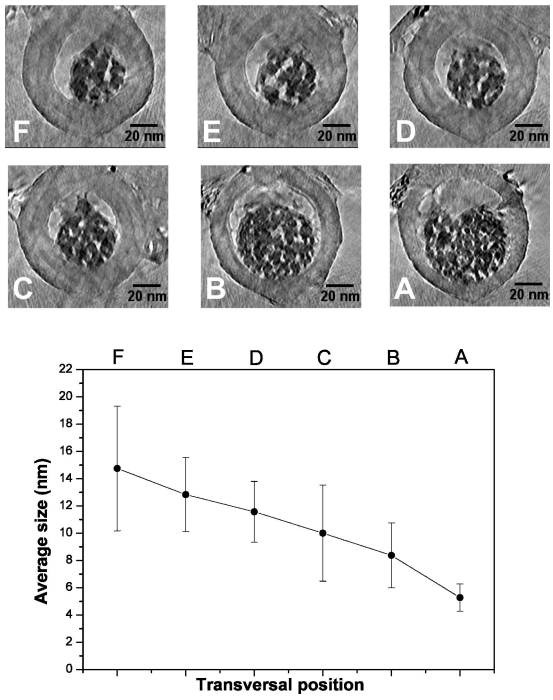

Figure 5. Above: Successive transverse sections through the reconstructed volume. The corresponding z-positions along the nanowire are indicated on the longitudinal section of Figure 3C. Below: Average size of the $CoFe_2O_4$ nanoparticles as a function of the position along the nanotube axis.

calcination step probably leads to a higher partial pressure which induces the growth of bigger particles (via a hydrothermal process). Indeed, in the works of Zhang et al.,[13] the $CoFe_2O_4$ nanoparticles prepared by the microemulsion technique and constituting free-standing nanorods exhibit a relatively homogeneous particle size regardless their location

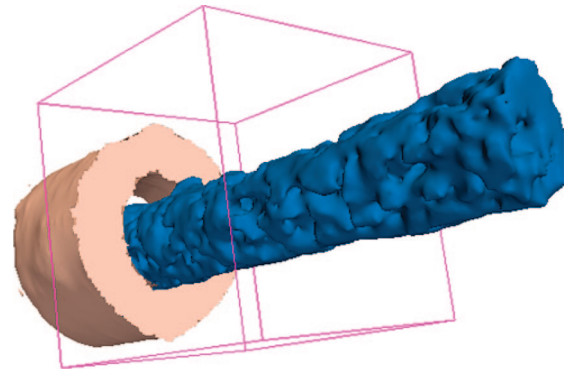

Figure 6. View of the 3D model obtained from the reconstructed volume showing the location and rough morphology of the $CoFe_2O_4$ nanowire (in blue) inside the carbon nanotube (in pink) channel as well as its highly porous structure.

along the longitudinal axis after a similar heat treatment. Such results could be explained by the fact that in this material the gaseous evacuation during the decomposition step was not restricted by the surrounding wall template. The average sizes of the $CoFe_2O_4$ particles deduced by 3D-TEM are similar to the sizes of the monocrystalline areas determined from HRTEM images (between 5 and 15 nm), as well as to the average particle size estimated by XRD. At this stage, we can propose a realistic model for the morphology of the nanowire: it contains monocrystalline particles with size ranging from 5 to 15 nm depending to their position with respect to the extremity of the tube. The monocrystallinity of the individual particles that comprise the nanowire is a key factor that can influence in a significant manner the magnetic behavior of the whole system.

Transverse sections through the reconstructed volume taken perpendicular to the $CoFe_2O_4$ nanowire are also accessible in Figure 5, which again illustrates the high porosity of the formed nanowire. A model of the reconstructed volume of the sample was calculated using a segmentation procedure based on gray-level intensities of the voxels (Figure 6). It clearly exhibits a cylindrical-like nanowire of $CoFe_2O_4$ with high porosity. This porosity can be easily calculated by means of the dedicated measurement software. By comparing the number of voxels corresponding to $CoFe_2O_4$ material to those located inside a cylindrical surface surrounding the nanowire, a residual porosity within the nanowire of about 38% was determined.

Moreover, by comparing the number of voxels corresponding to $CoFe_2O_4$ to those located within the internal surface of the nanotube, we can also deduce available information about the filling of the tube with magnetic material. To make this, we calculated successively the amount of $CoFe_2O_4$ and the corresponding available volume inside the tube, taking a unity length along the tube axis of 30 nm. The corresponding values are presented in Figure 7, and their ratio giving the filled fraction of the nanotube is almost constant along the tube axis and is about 50%.

It is noteworthy that the coercivities of the as-synthesized $CoFe_2O_4$ nanowires are relatively high, i.e., ca. 13500 Oe at 5 K, which could render them interesting for use as randomly oriented magnetic nanowires in the fabrication of flexible

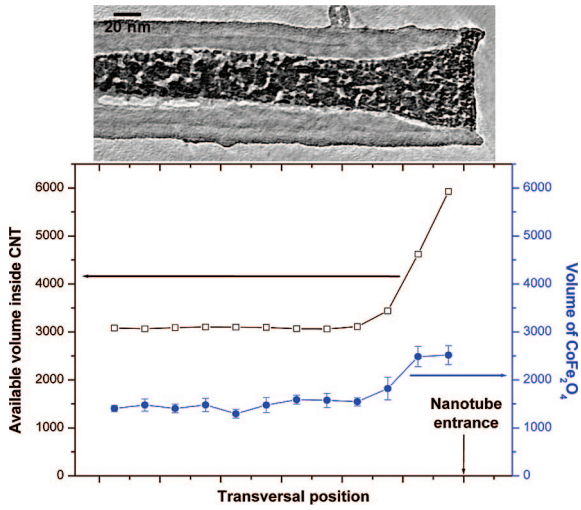

Figure 7. Available volume inside the CNT and the corresponding volume occupied by the $CoFe_2O_4$ nanowire as a function of the position along the nanotube axis.

magnets after blending them with polymers. Preliminary experiments carried out on the alignment under an external applied magnetic field of these magnetic centers were conducted, and the results are presented as Supporting Information (Figure SI5). According to the results, the CNT containing $CoFe_2O_4$ nanowires can be effectively aligned along the magnetic field inside a solution of polymer.

In summary, we have demonstrated here that the ability of TEM tomography to extract microstructural information permits deeper investigations on encapsulated nanostructured materials. Such detailed microstructural analysis was not accessible by means of conventional TEM imaging due to the strong overlapping in the projected images. It is thought that the microstructural study of such a complex sample could be applied to new materials in which the determination of the morphology and spatial organization is essential in order to understand and optimize the properties of interest for specific applications. By coupling the 3D-TEM and the HRTEM techniques, we have shown that the $CoFe_2O_4$ magnetic particle that compose the nanowire are monocrystalline and their size is closely dependent on the location of the particle within the nanotube, i.e., small particles close to the tube tip (5 nm) and bigger particles inside the tube channel (15 nm). Such phenomenon was attributed to the problem of local pressure linked with the evacuation of gaseous compounds inside a narrow and long nanoscopic channel during the liquid-to-solid transformation of the salt precursor solution into the $CoFe_2O_4$ nanowire. TEM tomography also revealed that the nanowire was constituted by several chain-like assemblies of nanoparticles almost parallel to the longitudinal axis. The surrounding nonmagnetic carbon wall, with low density compared to the one of the casted magnetic compounds, allows the avoidance of magnetic dipolar relaxation and aggregation that could trigger a significant lowering of the magnetization of the $CoFe_2O_4$. On the other hand, we showed that with this preparation method and for this internal diameter of the tube, the $CoFe_2O_4$ nanowire presented a continuous structure along the tube, has a residual porosity of 38%, and can fill the tube at only 50%, parameters which can influence in a significant manner the magnetic behavior of this system.

Work is ongoing in order to get more details about the nanowire growth mechanism as a function of the heat treatment and also to conduct theoretical correlation of the magnetic properties of the one-dimensional magnetic materials.

Acknowledgment. We thank A. Derory for performing magnetic measurements. Dr. Patrick Nguyen (Sicat SA) is also gratefully acknowledged for helpful discussions and participation in the $CoFe_2O_4$/CNT alignment in the polymer matrix.

Supporting Information Available: Zeta potential curves of the CNTs treated under different conditions as a function of the pH of the solution. TEM micrographs showing the selectivity of the deposition in the case of iron for two types of carbon nanotubes. XRD pattern of the $CoFe_2O_4$ nanowire after thermal treatment under Ar at 400 °C. Typical TEM image recorded in bright-field mode of the same sample showing a well defined and highly porous $CoFe_2O_4$ nanowire. Magnetization measurements performed on the sample. SEM micrograph of the $CoFe_2O_4$ nanowires/CNT channel after alignment in a polymeric matrix under external magnetic field. This material is available free of charge via the Internet at http://pubs.acs.org.

References

(1) Sun, S. *Adv. Mater.* **2006**, *18*, 393.
(2) Doyle, P. S.; Bibette, J.; Bancaud, A.; Viovy, J.-L. *Science* **2002**, *295*, 2237.
(3) Willner, I.; Katz, E. *Angew. Chem.* **2003**, *42*, 4576.
(4) Yoon, T.-J.; Yu, K. N.; Kim, E.; Kim, J. S.; Kim, B. G.; Yun, S.-H.; Sohn, B.-H.; Cho, M.-H.; Lee, J.-K.; Park, S. B. *Small* **2006**, *2*, 209.
(5) Pham-Huu, C.; Keller, N.; Estournes, C.; Ehret, G.; Greneche, J. M.; Ledoux, M. J. *Phys. Chem. Chem. Phys.* **2003**, *5*, 3716.
(6) Ji, G.; Tang, S.; Xu, B.; Gu, B.; Du, Y. *Chem. Phys. Lett.* **2003**, *379*, 484.
(7) Muramatsu, H.; Hayashi, T.; Kim, Y. A.; Shimamoto, D.; Endo, M.; Terrones, M.; Dresselhaus, M. S. *Nano Lett.* **2008**, *8*, 1, 237.
(8) Hu, J.; Bando, Y.; Zhan, J.; Zhi, C.; Golberg, D. *Nano Lett.* **2006**, *6*, 1136. 6.
(9) Elias, A. L.; Rodriguez-Manzo, J. A.; McCartney, M. R.; Golberg, D.; Zamudio, A.; Baltazar, S. E.; Lopez-Urias, F.; Munoz-Sandoval, E.; Gu, L.; Tang, C. C; Smith, D. J.; Bando, Y; Terrones, H.; Terrones, M. *Nano Lett.* **2005**, *3*, 467. 5.
(10) Sloan, J.; Kirkland, A. I; Hutchison, J. L.; Green, M. L. H. *Chem. Commun.* **2002**, *13*, 1319.
(11) Elias, A. L.; Rodriguez-Manzo, J. A.; McCartney, M. R.; Golberg, D; Zamudio, A.; Baltazar, S. E.; Lopez-Urias, F.; Munoz-Sandoval, E.; Gu, L.; Tang, C.; Smith, D. J; Bando, Y; Terrones, H.; Terrones, M. *Nano Lett.* **2005**, *3*, 467. 5.
(12) Keller, N.; Pham-Huu, C.; Shiga, T.; Estournes, C.; Greneche, J. M.; Ledoux, M. J *J. Magn. Magn. Mater.* **2004**, *272–276*, 1642.
(13) Zhang, Z.; Rondinone, A. J.; Ma, J. X.; Shen, J.; Dai, S. *Adv. Mater.* **2005**, *17*, 1415.
(14) Janssen, A. H.; Koster, A. J.; De Jong, K. P. *J. Phys. Chem. B* **2002**, *106*, 11905.
(15) de Jong, K. P.; Koster, A. J. *ChemPhysChem* **2002**, *3*, 776.
(16) Weyland, M.; Midgley, P. A. *Mater. Today* **2004**, *7*, 32.
(17) de Jong, K. P.; Koster, A. J.; Janssen, A. H.; Ziese, U. *Stud. Surf. Sci. Catal.* **2005**, *157*, 225.
(18) Weyland, M.; Yates, T. J. V.; Dunin-Borkowski, R. E.; Laffont, L.; Midgley, P. A. *Scr. Mater.* **2006**, *55*, 29.
(19) Ersen, O.; Werckmann, J.; Houllé, M.; Ledoux, M. J.; Pham-Huu, C *Nano Lett.* **2007**, *7*, 1898.

(20) Koster, A. J.; Ziese, U.; Verkleij, A. J.; Janssen, A. H.; de Jong, K. P. *J. Phys. Chem. B* **2000**, *104*, 9368.
(21) Midgley, P. A.; Weyland, M.; Thomas, J. M.; Johnson, B. F. G. *Chem. Commun.* **2001**, *10*, 907.
(22) Wang, Z. H.; Choi, C. J.; Kim, B. K.; Kim, J. C.; Zhang, Z. D. *Carbon* **2003**, *41*, 1751.
(23) Dong, X. L.; Zhang, Z. D.; Chuang, Y. C.; Jin, S. R. *Phys. Rev. B* **1999**, *60*, 3017.
(24) Sun, X.; Gutierrez, A.; Yacaman, M. J.; Dong, X.; Jin, S. *Mater. Sci. Eng., A* **2000**, *286*, 157.
(25) Mastronarde, D. N. *J. Struct. Biol.* **1997**, *120*, 343.
(26) Weyland, M. *Top. Catal.* **2002**, *21*, 175.
(27) Esumi, K.; Ishigami, M.; Nakajima, A.; Sawada, K.; Honda, H. *Carbon* **1996**, *34*, 279.
(28) Kim, B.; Sigmund, W. *Langmuir* **2004**, *20*, 8239.
(29) Hu, H.; Yu, A.; Kim, E.; Itkis, M. E.; Bekyarova, E.; Haddon, R. C. *J. Phys. Chem. B* **2005**, *109*, 11520.
(30) Vaisman, L.; Marom, G.; Wagner, H. D. *Adv. Funct. Mater.* **2006**, *16*, 357.
(31) Kim, D.-H.; Kim, K.-M.; Kim, K.-N.; Shim, I.-B; Lee, Y.-K. *Technical Proceedings of the 2007 NSTI Nanotechnology Conference and Trade Show*; CRC Press: Boca Raton, FL, 2007; Vol. 2, 748−751.
(32) Slawska-Waniewska, A.; Didukh, P.; Greneche, J. M.; Fannin, P. C. *J. Magn. Magn. Mater* **2000**, *215–216*, 227.
(33) Shi, Y.; Ding, J.; Yin, H. *J. Alloys Compd.* **2000**, *308*, 290–295.
(34) Kim, Y. I.; Kim, D.; Lee, C. S. *Physica B* **2003**, *337*, 42–51.
(35) Lee, S. W.; Kim, C. S. *J. Magn. Magn. Mater.* **2006**, *303*, e315–e317.
(36) Calero-DdelC, V. L.; Rinaldi, C. *J. Magn. Magn. Mater.* **2007**, *314*, 60–67.
(37) Ahn, Y.; Choi, E. J.; Kim, S.; Ok, H. N. *Mater. Lett.* **2001**, *50*, 47.
(38) Song, Q.; Zhang, Z. J. *J. Am. Chem. Soc.* **2004**, *126*, 6164.
(39) Ammar, S.; Helfen, A.; Jouini, N.; Fievet, F.; Rosenman, I.; Villain, F.; Molinié, P.; Danot, M. *J. Mater. Chem.* **2001**, *11*, 186.
(40) Jeppson, P.; Sailer, R.; Jarabek, E.; Sandstrom, J.; Anderson, B.; Bremer, M.; Grier, D. G.; Schulz, D. L.; Caruso, A. N.; Payne, S. A.; Eames, P.; Tondra, M.; He, H.; Chrisey, D. B. *J. Appl. Phys.* **2006**, *100*, 114324.
(41) Maaz, K.; Mumtaz, A.; Hasanain, S. K.; Ceylan, A. *J. Magn. Magn. Mater.* **2007**, *308*, 289.
(42) Muroi, M.; Street, R.; McCormick, P. G.; Amighian, J. *Phys. Rev.* **2001**, *63*, 184414.
(43) Hart, R. G.; Yoshiyama, J. M. *Proc. Natl. Acad. Sci. U.S.A.* **1970**, *5*, 402.

NL072714E